A Multi-Resolution Preconditioner for Non-Conformal Meshes in the MoM Solution of Large Multi-Scale Structures

A Multi-Resolution Preconditioner for Non-Conformal Meshes in the MoM Solution of Large Multi-Scale Structures

V. F. Martin *Member, IEEE*, J. M. Taboada *Senior Member, IEEE* and F. Vipiana *Senior Member, IEEE*

***Abstract*— The paper presents a multi-resolution preconditioner able to improve the solution convergence, via the method of moments and the multilevel fast multipole algorithm, in the case of non-conformal meshes applying the multi-branch Rao-Wilton-Glisson basis functions. The proposed preconditioner enables, for the first time, an automatic multi-level quasi-Helmholtz decomposition on non-conforming meshes, including also the generation of the topological (global) loop functions. Moreover, the generation of the proposed preconditioning scheme is fully parallelized in a multicore shared-memory enviroment. Numerical results show the great flexibility of this approach for the solution of electrically-large multi-scale objects including h-refinement discretizations.**

***Index Terms*— Multi-resolution preconditioner, multi-branch Rao-Wilton-Glisson basis functions, quasi-Helmholtz decomposition, method of moments, multilevel fast multipole algorithm, fast solvers.**

I. Introduction

The extension of the surface integral equations (SIEs) [1]–[10] to non-conforming meshes has ignited intense research in the last years, with the goal of finding versatile and accurate methodologies to address large and multi-scale complex problems, while simplifying the otherwise necessary computer-aided-design (CAD) generation and meshing processes.

Moreover, the extremely different levels of details depending on the working frequencies and the proper addressing of the geometrical issues tends to greatly increase the number of unknowns when leading with real life problems. In this context, h-refinement techniques work to develop methods capable of incresing the accuracy of the SIE solution for coarse-meshed multiscale problems through local mesh refinement [11].

Discontinuous Galerkin (DG) implementations of the SIEs [12]–[17], based on the combination of the half-Rao-Wilton-Glisson (h-RWG) basis functions with an interior penalty (IP) term, are one of the most popular approaches to deal with this kind of problems. The key to these methods lies in the careful treatment of charge accumulation at the (non-conforming) boundaries between the h-RWG basis functions. These implementations are made through the incorporation of an IP and the appropriate selection of a stabilization parameter, closely related to the triangular mesh size. Other non-conforming SIE schemes alternative to DG that avoid the inclusion of an IP term (and the involved singular integrals) are the monopolar-RWG basis functions [18]–[23], based on the addition of artificial testing surfaces or the use of volumetric testing integrals.

More recently, a different approach has been introduced that is based on the use of the so-called multi-branch RWG (MB-RWG) basis functions [24]. These functions are defined over non-conforming triangles sharing a common tearing line, with the only restriction that the nodes of the coarser mesh at the tearing line are consistent with part of the nodes of the finer mesh (i.e, the mesh must be partially node-conforming). This type of meshing is the one emerging after h-refinements, so the MB-RWG basis functions are especially suited to this problem. Moreover, they also bring other advantages. In particular, they can be easily integrated into existing RWG-based SIE codes without the need of including penalty terms, additional volumetric integrals or artificial surfaces, while still simplifying the CAD and mesh generation. Additionally, MB-RWG are div-conforming functions, which has allowed the derivation of loop (solenoidal) bases as linear combination of them [25].

Regardless of the meshing and basis functions applied, it is well-known that SIE methods suffer from ill-conditioning when applied to realistic high-fidelity models that include multi-scale features, making their resolution challenging. The use of physics-based preconditioners allows to significantly improve the convergence and iteration count in these problems, taking advantage of their physical properties. Some examples of dense-discretization stable physics-based preconditioners are the Calderón preconditioner [6], [26]–[31] or the multi-resolution (MR) preconditioner [8], [32]–[37]. In the latter, a set of multi-level basis functions is introduced to discretize the problem while keeping the different scales of variation of the solution [38], [39]. This preconditioner improves the spectral properties and conditioning of the original method of moments (MoM) system matrix [40], especially in the case of multi-scale structures, by virtue of a quasi-Helmholtz decomposition in which the unknown current is separated into

This work is part of the R&D project PID2020-116627RB-C21/22, funded by Ministerio de Ciencia e Innovación (MCIN/AEI/10.13039/501100011033). This work was also supported by Spanish government (TEC2017-85376-C2-1-R, TEC2017-85376-C2-2-R, FPU00550/17, EST21/00590), Extremadura Regional Government and European Union FEDER (GR18055, GR21072, IB18073). The contribution of V. F. Martin is also supported by Spanish government and the European recovery fund Next Generation EU under Project MS-26 (RD 289/2021 Margarita Salas UEx).

V. F. Martin and J. M. Taboada are with the Departamento de Tecnología de los Computadores y Comunicaciones, Universidad de Extremadura, Spain, (e-mail: vfmartin@unex.es, tabo@unex.es).

V. F. Martin and F. Vipiana are with the Department of Electronics and Telecommunications, Politecnico di Torino, 10129 Torino, Italy (e-mail: francesca.vipiana@polito.it).

its solenoidal and non-solenoid parts. However, despite recent efforts to improve the capabilities of DG-SIE methods, to date the application of physics-based preconditioners is limited to conforming schemes such as those relying on the use of RWG basis functions. This is, in part, due to the non div-conforming properties of the h-RWG functions.

In this context, the use of a set of div-conforming functions defined over (possibly) non-conforming meshes and combined with physics-based preconditioners would bring a very appealing advantage, posing a good compromise between performance and versatility in electromagnetic modelling of complex geometries with multi-scale features.

In this paper, we focus on the application of a multilevel quasi-Helmholtz decomposition for non-conformal meshes. To address it, the MR preconditioner is developed over the multi-branch RWG basis functions and applied to the MoM solution of complex multi-scale problems discretized with non-conformal meshes and accelerated via the multilevel fast multipole algorithm (MLFMA). The resulting formulation provides an alternative to automatically build a multilevel quasi-Helmholtz decomposition into solenoidal and non-solenoidal functions on this kind of non-conformal meshes, and completely avoids the awkward topological (global) loop functions searching, because they are automatically obtained. The proposed MR-MB scheme is actually a multiplicative preconditioner that can be easily inserted into any fast MoM-based code. In this work, the proposed preconditioner is applied to the Combined Field Integral Equation (CFIE) for closed surfaces and to the Electric Field Integral Equation (EFIE) for open surfaces for the solution of scattering and radiation problems. Numerical examples demonstrate the versatility and performance of this scheme. To the authors' knowledge, this is the first work where a multi-level quasi-Helmholtz decomposition is applied to non-conforming meshes in SIE. Preliminary results were recently presented in [41], [42]

The rest of the paper is organized as follows. The formulation background is presented in Sect. II. Section III illustrates the MR generation scheme for MB-RWG functions. The numerical results are in Sect. IV to validate and illustrate the flexibility of the proposed method with different challenging realistic structures. Finally, some concluding remarks are drawn in Sect. V.

II. Background

In this section the definition of the multi-branch RWG basis functions is summarized and the proposed SIE formulation is described in order to set up the notation.

A. Multi-Branch RWG Basis Functions

The RWG basis functions [43] are the basis functions par excellence for solving SIEs problems defined in terms of triangular meshes. They are defined over two domains (namely, the positive and negative triangles) and have well-known properties that make them especially suitable for solving integral equation problems. Analogous to the RWG functions, the MB-RWG functions [24] are defined over a positive and a negative domain, but, in this case, one of the two

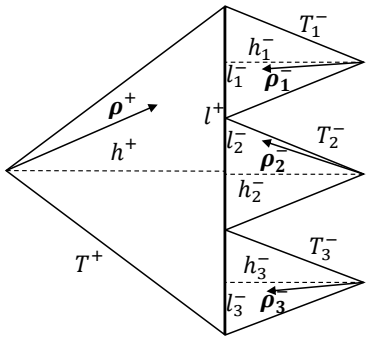

Fig. 1. Example of an MB-RWG basis function with three branches.

domains (which without loss of generality we will consider here to be the negative one) can be made up of several adjacent triangles (as shown in Fig. 1), instead of a single one, as:

$$\mathbf{f}_n^{\mathrm{MB}}(\mathbf{r}) = \begin{cases} \frac{\boldsymbol{\rho}_n^+}{h_n^+}, & \text{with } \mathbf{r} \in T_n^+ \\ -\frac{\boldsymbol{\rho}_{n,i}^-}{h_{n,i}^-}, & \text{with } \mathbf{r} \in T_{n,i}^-,\ i = 1, \ldots, M_n \\ 0, & \text{otherwise} \end{cases} \tag{1}$$

where T_n^+ is the positive triangle, and $T_{n,i}^-$ are the M_n triangles in the negative domain of the n-th MB-RWG basis function; $\boldsymbol{\rho}_n$ and h_n are the position vector relative to the free vertex and the height relative to the common edge of each triangle, respectively. The MB-RWG functions thus defined keep all the desirable properties of RWG functions, namely, null normal component around the outer edges, unit normal component at the common edge lines, and a divergence that can be analytically evaluated as

$$\nabla \cdot \mathbf{f}_n^{\mathrm{MB}}(\mathbf{r}) = \begin{cases} \frac{2}{h_n^+}, & \text{with } \mathbf{r} \in T_n^+ \\ -\frac{2}{h_{n,i}^-}, & \text{with } \mathbf{r} \in T_{n,i}^-, i = 1, \ldots, M_n \\ 0, & \text{otherwise} \end{cases} \tag{2}$$

B. CFIE-MoM Formulation

We consider a perfect electric conductor (PEC) body in a homogeneous background with equivalent electric current densities $\mathbf{J}(\mathbf{r}')$ defined on its surface S. Applying the equivalence principle to the total electric and magnetic fields, the tangential electric field integral equation (T-EFIE) and the normal magnetic field integral equation (N-MFIE) can be obtained as follows:

$$\text{T-EFIE: } \eta \mathcal{L}\left\{\mathbf{J}\right\}_{\tan} = \mathbf{E}_{\tan}^{\mathrm{inc}} \tag{3}$$

$$\text{N-MFIE: } \hat{n} \times \mathcal{K}\left\{\mathbf{J}\right\} + \frac{1}{2}\mathbf{J} = \hat{n} \times \mathbf{H}^{\mathrm{inc}} \tag{4}$$

where η is the intrinsic impedance of the background, $\hat{n}$ is the unit vector normal to the body surface and pointing to the background, and $\mathbf{E}^{\mathrm{inc}}$ and $\mathbf{H}^{\mathrm{inc}}$ are the incident electric and magnetic fields, respectively. The integro-differential operators $\mathcal{L}$ and $\mathcal{K}$ are defined as

$$\mathcal{L}\left\{\mathbf{J}\right\} \quad = \quad jk \iint_S \mathbf{J}(\mathbf{r}') g(\mathbf{r}, \mathbf{r}') dS' +$$

$$-\frac{1}{jk}\nabla\iint_S \mathbf{J}(\mathbf{r}')\nabla' g(\mathbf{r},\mathbf{r}')\,dS' \quad (5)$$

$$\mathcal{K}\{\mathbf{J}\} = PV\iint_S \mathbf{J}(\mathbf{r}')\times\nabla' g(\mathbf{r},\mathbf{r}')\,dS'. \quad (6)$$

where k is the wavenumber, and $\mathbf{r}$ and $\mathbf{r}'$ are the observation and source point, respectively; ∇' denotes the divergence in the primed (source) coordinates, and PV the principal value of the integral in (6). The homogeneous Green's function $g(\mathbf{r},\mathbf{r\prime})$ is defined as

$$g(\mathbf{r},\mathbf{r}') = \frac{e^{-jk|\mathbf{r}-\mathbf{r}'|}}{4\pi|\mathbf{r}-\mathbf{r}'|}. \quad (7)$$

The combined field integral equation (CFIE) can be derived from the above integral equations as:

$$\text{CFIE} = \alpha\frac{\text{T-EFIE}}{\eta} + (1-\alpha)\ \text{N-MFIE} \quad (8)$$

where $0<\alpha<1$ is the weight controlling the contribution of the EFIE and MFIE equations, which is selected to 0.5 in this work.

To obtain the equivalent electric current densities $\mathbf{J}$ on the PEC object surface, the conventional MoM procedure is applied to (8). The current densities on the whole body are expanded into a sum of N known vector basis functions $\mathbf{f}_n$ in the form

$$\mathbf{J} = \sum_{n=1}^{N} I_n \mathbf{f}_n \quad (9)$$

with I_n being the unknown expansion complex coefficients. Substituting (9) into (8) and applying the Galerkin testing procedure, a system of linear equations is derived from the integral equations and can be expressed as a dense matrix system as follows:

$$[Z]\,[I] = [V] \quad (10)$$

with

$$[Z] = \left(\alpha\left[Z^{\text{EFIE}}\right] + (1-\alpha)\left[Z^{\text{MFIE}}\right]\right) \quad (11)$$

where $\left[Z^{\text{EFIE}}\right]$ and $\left[Z^{\text{MFIE}}\right]$ are a $N\times N$ matrices, containing the coupling between all the basis and testing functions, $[I]$ is an N-column vector collecting the unknown coefficients I_n of the current expansion, and $[V]$ is the N-column excitation vector, closely related to the incident fields originated by the sources. Each m,n element of the $\left[Z^{\text{EFIE}}\right]$ and $\left[Z^{\text{MFIE}}\right]$ matrices, with m and $n=1,\ldots,N$, can be expanded as follows:

$$\begin{aligned} Z^{\text{EFIE}}_{mn} &= \iint_{\Delta_m}\mathbf{f}_m\cdot\mathcal{L}\{\mathbf{f}_n\}\,dS \\ &= \iint_{\Delta_m}\mathbf{f}_m\cdot\iint_{\Delta_n}\mathbf{f}_n\,g(\mathbf{r},\mathbf{r}')dS'dS + \\ &+ \frac{1}{jk}\iint_{\Delta_m}\mathbf{f}_m\cdot\nabla\iint_{\Delta_n}\mathbf{f}_n\cdot\nabla' g(\mathbf{r},\mathbf{r}')dS'dS \quad (12) \\ Z^{\text{MFIE}}_{mn} &= \iint_{\Delta_m}\mathbf{f}_m\cdot\hat{n}\times\mathcal{K}\{\mathbf{f}_n\}\,dS + \frac{1}{2}\iint_{\Delta_m}\mathbf{f}_m\cdot\mathbf{f}_n dS \\ &= \iint_{\Delta_m}\mathbf{f}_m\times\hat{n}\cdot\iint_{\Delta_n}\mathbf{f}_n\times\nabla g(\mathbf{r},\mathbf{r}')dS'dS + \\ &+ \frac{1}{2}\iint_{\Delta_m}\mathbf{f}_m\cdot\mathbf{f}_n dS \quad (13) \end{aligned}$$

where Δ_m and Δ_n denote the subdomain where the functions $\mathbf{f}_m$ and $\mathbf{f}_n$ are defined, respectively. Equation (12) involves hyper-singular integrals, whose singularity order can be reduced in terms of the product rule for divergence and the divergence Gauss theorem, by transferring the gradient operators from the Green's function and the source (inner) integral to the divergence of the basis and testing functions.

III. Multi-Resolution Multi-Branch (MR-MB) Preconditioner

The multi-resolution (MR) preconditioner improves the spectral properties and condition number of the original MoM system matrix thanks to a multi-level quasi-Helmholtz decomposition of the induced currents, splitting them into their solenoidal and non-solenoidal parts [44].

The standard MR generation procedure is summarized here. First, the input triangular mesh, supporting the discretization of the problem in terms of standard basis functions (i.e., RWG basis functions), is rearranged until getting a set of meshes with different mesh-element (namely, cell) sizes. This is done via a multi-level algorithm in which the adjacent cells of the previous level, starting from level-0 triangular input facets, are aggregated, giving rise to macro-cells. Then, generalized basis functions (i.e., generalized RWG basis functions) are defined on each pair of adjacent macro-cells, and, from them via a local singular value decomposition (SVD) procedure, the solenoidal and non-solenoidal MR basis functions are obtained. The above scheme is applied recursively up to the quasi-Nyquist (coarsest) cell-size level, where generalized RWGs are defined completing the set of multi-level basis functions [8], or up to when one last-level macro-cell completely includes all the analyzed structure [32]. It is important to remark that generated MR and generalized RWG basis functions at any level can be described as linear combinations of the initial underlying functions (i.e., the standard RWG basis functions), and hence the MR preconditioner can be applied to the MoM system matrix via a simple matrix multiplication as any algebraic preconditioner.

In the following sections the MR generation scheme will be detailed in the case of non-conformal meshes where MB-RWG basis functions are defined.

A. Multilevel mesh grouping algorithm

One of the critical points regarding the computational efficiency of the MR preconditioner is the development of a cell grouping algorithm that allows to keep a low complexity in applying the local SVDs needed to split the underlying currents into their solenoidal and non-solenoidal parts. The grouping strategy described here extends the scheme proposed in [45] to non-conformal triangular meshes.

The procedure is approached through an iterative scheme repeated level by level, in which central cells are selected and merged together with their neighbors (connected or adjacent cells), leading to the macro-cells of the next level. It is designed to optimize some qualitative aspects of the cells

formed, in order to guarantee a good overall performance in the application of the MR preconditioner. These objectives are mainly to maximize aggregation in macro-cells and prevent the formation of holes (multiply-connected cells, e.g. ring-like cells that enclose another cell). They can be achieved by addressing the central cell selection criteria in terms of specific metrics defining different distances between cells. It is worth mentioning that such scheme provides improved performance compared to other grouping strategies (such as octree-based clustering schemes), posing a good balance in the number of child cells throughout the multilevel cluster regardless of the density of the underlying mesh, while keeping the number of elements of the local SVDs independent of the number of unknowns. This results in a complexity of $O(N \log N)$ for the generation of MR basis functions, with N equal to the total number of unknowns, as shown in Sect. III-D.

Nevertheless, in the case of non-conformal or partially non-conformal meshes supporting MB-RWG basis functions, some additional constraints are required to ensure charge conservation in emerging macro-cells. Such constraints are addressed here through the specific treatment of the non-conformal input mesh (at initial, level-0), where both RWGs and MB-RWGs are defined, posing a proper definition of the level-1 generalized basis functions. In particular, during the aggregation procedure at level-0, if a triangle belonging to the negative domain of an MB-RWG function (see Fig. 1) is aggregated, then all negative triangles of that domain must also be merged into the same level-1 macro-cell, which ensures that each level-1 generalized basis function can be described as a linear combination of complete level-0 RWG and/or MB-RWG functions. Additionally, all triangles with a vertex belonging to the internal nodes of this MB-RWG must also be aggregated in the same macro-cell. The above constraints guarantee conservation of charge at each level.

To better illustrate the described procedure, Fig. 2 gathers all the possible (five) different grouping alternatives when MB-RWG functions come into play, depending on the position of the central triangle picked to make the grouping. The five cases are described as consecutive iterations of the proposed algorithm. Let us first consider a central triangle belonging to the positive domain of an MB-RWG function, in this case C_1^0 in Fig. 2(a), which belongs to the positive domain of f_1^0. A level-1 macro-cell is created by merging this central triangle together with its neighbours (connected triangles), two corresponding to RWG domains (C_9^0 and C_{10}^0) and four corresponding to the negative part of MB-RWG f_1^0 ($C_2^0 - C_5^0$). Taking into account the constraints appointed above, since the negative part of an MB-RWG is being aggregated to a macro-cell, all triangles with a vertex belonging to the internal nodes of f_1^0 ($C_6^0 - C_8^0$) should also be merged into the new macro-cell, labeled C_1^1 in Fig. 2(b).

Let us now consider the case of a central triangle belonging to the negative domain of an MB-RWG, in this case C_{13}^0, which belongs to the negative domain of f_2^0. A level-1 macro-cell is formed by merging this central triangle with its neighbours (C_{11}^0, C_{16}^0 and C_{17}^0). Considering now that C_{13}^0 belongs to the negative part of an MB-RWG, all negative triangles ($C_{12}^0 - C_{15}^0$) and all those triangles connected to the internal nodes of f_2^0 ($C_{16}^0 - C_{18}^0$) must also be merged, resulting in the new macro-cell labeled C_2^1 in Fig. 2(b).

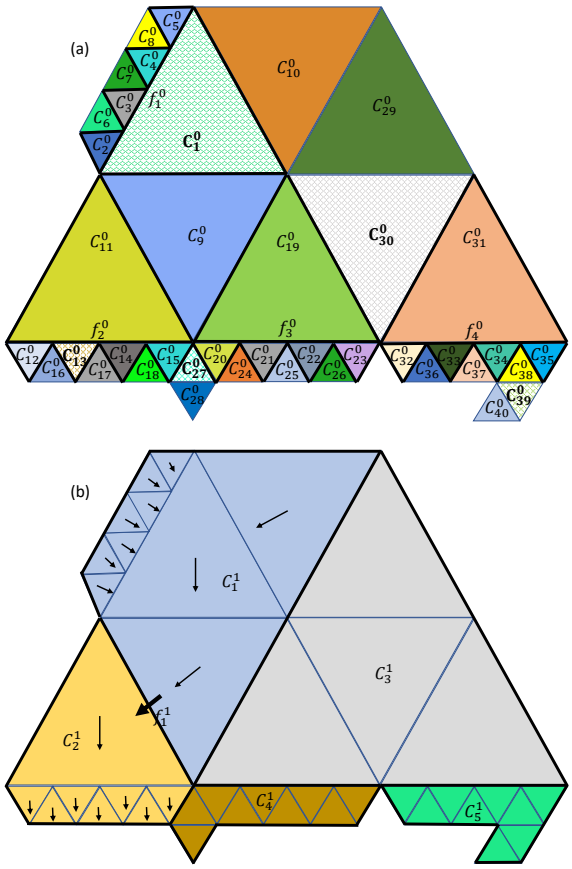

Fig. 2. Example of cell grouping. (a): level-0 mesh including three MB-RWGs; (b): level-1 mesh (each macro-cell corresponds to a group of adjacent triangles with the same color) with an example of a generalized MB-RWG defined on level-1 cells labelled with "C_1^1" and "C_2^1"

We next consider the triangle C_{30}^0, which does not belong to an MB-RWG, as the central triangle. The adjacent triangles C_{19}^0 and C_{31}^0, belonging to respective positive domains of the MB-RWG basis functions f_3^0 and f_4^0, as well as triangle C_{29}^0, belonging to a conventional RWG, are aggregated to the macro-cell labeled C_3^1 in Fig 2(b). In this case, the negative triangles of the MB-RWG functions f_3^0 and f_4^0 remain free and will be added in subsequent iterations of the algorithm.

A different case of central triangle not belonging to an MB-RWG function is that of triangle C_{27}^0. Similarly to previous cases, a new macro-cell is created by merging this triangle with its neighbours (C_{20}^0 and C_{28}^0). Note that C_{15}^0 cannot be included here as this triangle has been merged in a previous iteration of the algorithm and already belongs to a level-1 macro-cell. As C_{20}^0 belongs to the negative domain of an MB-RWG (function f_3^0), triangles $C_{21}^0 - C_{23}^0$, as well as those connected to the internal nodes of f_3^0, $C_{24}^0 - C_{26}^0$, must be assigned to the same macro-cell, namely macro-cell C_4^1 in Fig 2(b).

As a final case, let us consider the selected central triangle C_{39}^0, which does not belong to an MB-RWG. A new macro-cell is created by merging this triangle with its neighbours

(C_{38}^0 and C_{40}^0). Since triangle C_{38}^0 is connected to an internal node of MB-RWG function f_4^0, all triangles connected to the internal nodes of f_4^0 ($C_{36}^0 - C_{38}^0$), together with all negative triangles of f_4^0 ($C_{32}^0 - C_{35}^0$), must be included in the same macro-cell, thus leading to macro-cell C_5^1.

As verified in the Sects. III-D and IV, despite the additional constrains needed to consider non-conformal meshes, the algorithm described above maintains the original complexity of the multi-resolution generation procedure applied to realistic non-conformal problems.

The algorithm described above is then applied to the rest of the levels, but without the need to consider non-conforming constraints at higher levels. Depending on the electrical-size of the discretized structure, the scheme is applied until the quasi-Nyquist (coarsest) cell-size level, or up to when all level-(L–1) cells are completely included in one level-L cell only, allowing an automatic multilevel quasi-Helmholtz decomposition for the first time applied to non-conforming meshes.

B. Generalized MB-RWG Basis Functions

A set of generalized basis functions (gf) $\mathbf{f}_i^l$ is defined on each pair of adjacent level-l generalized cells $C_i^{l,+}$ and $C_i^{l,-}$ and described as linear combination of the level-$(l-1)$ functions as follows:

$$\mathbf{f}_i^l(\mathbf{r}) = \sum_{n=1}^{N_i^{l-1}} f_{i,n}^l \mathbf{f}_{\mu_i(n)}^{l-1}(\mathbf{r}),$$
$$[\mu_i] = \left[j = j_1, \ldots, j_{N_i^{l-1}} / \mathbf{f}_j^{l-1}(\mathbf{r}) \in C_i^{l,+} \cup C_i^{l,-} \right] \quad (14)$$

where N_i^{l-1} is the number of level-$(l-1)$ functions defined strictly within the $\mathbf{f}_i^l(\mathbf{r})$ domain. An example of generalized MB-RWG function is shown in Fig. 2(b) defined on two level-1 cells.

This set of generalized bases reproduces the behavior of the initial MB-RWG and RWG basis functions at each level. In order to find the coefficients $f_{n,i}^l$ of the above expansion, the surface divergence operator $\nabla_s \cdot$ is applied to both sides of (14), and the resulting equation is projected onto the cells of level-$(l-1)$, posing the following linear system:

$$\left[Q_i^l\right] \left[f_i^l\right] = \left[q_i^l\right] \quad (15)$$

where $\left[Q_i^l\right]$ is a $M_i^{l-1} \times N_i^{l-1}$ matrix, called charge matrix, whose each m, n element is defined as

$$Q_{im,n}^l = \langle\, p_m^{l-1}, \nabla_s \cdot \mathbf{f}_{\mu_i n}^{l-1}(\mathbf{r}) \rangle \quad (16)$$

with M_i^{l-1} equal to the number of level-$(l-1)$ cells that uniquely define the domain of each $\mathbf{f}_i^l$ function, and p_m^{l-1} corresponding to a pulse function, equal to unity inside the corresponding level-$(l-1)$ cell, C_m^{l-1}, and zero elsewhere. $\left[f_i^l\right]$ is a N_i^{l-1} column vector that collects the coefficients $f_{i,n}^l$ with $n = 1, \ldots, N_i^{l-1}$, and $\left[q_i^l\right]$ is a M_i^{l-1} column vector whose elements elements are defined as

$$q_{im}^l = \langle\, p_m^{l-1}, \nabla_s \cdot \mathbf{f}_i^l(\mathbf{r}) \rangle. \quad (17)$$

To facilitate the generation of the above set of generalized functions, in the original MR generation scheme [32] the standard RWG functions defined on the input triangular mesh are normalized by the corresponding length of the common edge, as

$$\mathbf{f}_{i,RWG}^0(\mathbf{r}) = \begin{cases} \frac{\boldsymbol{\rho}_i^+}{2A_i^+}, & \text{with } \mathbf{r} \in T_i^+ \\ -\frac{\boldsymbol{\rho}_i^-}{2A_i^-}, & \text{with } \mathbf{r} \in T_i^- \\ 0, & \text{otherwise} \end{cases} \quad (18)$$

with its correspond divergence as

$$\nabla_s \cdot \mathbf{f}_{i,RWG}^0(\mathbf{r}) = \begin{cases} \frac{1}{A_i^+}, & \text{with } \mathbf{r} \in T_i^+ \\ -\frac{1}{A_i^-}, & \text{with } \mathbf{r} \in T_i^- \\ 0, & \text{otherwise} \end{cases} \quad (19)$$

where A_i^+ and A_i^- are the areas of the positive and negative domain triangle, T_i^+ and T_i^-. Substituting (19) into (16) and (17), we obtain

$$Q_{im,n}^l = \begin{cases} \pm 1, & \text{if } C_m^{l-1} \equiv C_n^{l-1,\pm} \\ 0, & \text{otherwise} \end{cases} \quad (20)$$

$$q_{im}^l = \pm \frac{A_m^{l-1}}{A_i^{l,\pm}} \quad (21)$$

The above normalization allows easy definition of the charge system. The new elements of the charge matrix only contain "± 1 "or "0 "values, depending on the cells where each generalized function is defined. It also allows to calculate the divergence of a generalized function without worrying about the length of the common edge, which is often difficult to obtain for higher levels.

In the case of MB-RWG functions defined on non-conformal meshes, the standard functions defined on the input triangular mesh can be normalized by the corresponding length of the common edge of the positive triangle $l_{i,+}$, as

$$\mathbf{f}_{i,MB}^0(\mathbf{r}) = \begin{cases} \frac{\boldsymbol{\rho}_i^+}{2A_i^+}, & \text{with } \mathbf{r} \in T_i^+ \\ -\frac{l_{i,j}}{l_i^+} \frac{\boldsymbol{\rho}_{i,j}^-}{2A_{i,j}^-}, & \text{with } \mathbf{r} \in T_{i,j}^-,\ j = 1, \ldots, M_i \\ 0, & \text{otherwise} \end{cases} \quad (22)$$

where $A_{i,j}^-$ are the areas of the negative triangles $T_{i,j}^-$, $l_{i,j}$ are the edges of the negative triangles in common with T_i^+, and M_i is the number of negative triangles in the $\mathbf{f}_{i,MB}^0$ domain. Then, the divergence of (22) can be written as

$$\nabla_s \cdot \mathbf{f}_{i,MB}^0(\mathbf{r}) = \begin{cases} \frac{1}{A_i^+}, & \text{with } \mathbf{r} \in T_i^+ \\ -\frac{l_{i,j}}{l_i^+} \frac{1}{A_{i,j}^-}, & \text{with } \mathbf{r} \in T_{i,j}^-,\ j = 1, \ldots, M_i \\ 0, & \text{otherwise} \end{cases} \quad (23)$$

In these cases, the elements of the charge matrix $\left[Q_i^l\right]$ relative to negative triangles of an MB-RWG contain the relationship between the length of the negative and positive triangles. It is important to note that this fact is only present in the generation of the generalized functions defined on level-1, thus edges length only come into play in level-0 charge systems describing charge conservation in MB-RWG basis functions.

Once the charge matrices are properly defined, the coefficients of the generalized functions can be easily obtained at each level by solving the matrix system (15). But taking into account that the matrix system (15) is indeterminate [32], a new matrix system can be defined by reducing a random row and adding the condition that solenoidal currents do not contribute to the generalized function considered:

$$\begin{bmatrix} \widetilde{[Q_i^l]} \\ [U_i^l] \end{bmatrix} \left[f_i^l\right] = \begin{bmatrix} \widetilde{[q_i^l]} \\ [0] \end{bmatrix} \tag{24}$$

where $\widetilde{[Q_i^l]}$ and $\widetilde{[q_i^l]}$ correspond to $[Q_i^l]$ and $[q_i^l]$ with one row removed, respectively, $[U_i^l]$ is the set of right singular vectors in the null space of $[Q_i^l]$ (which corresponds to the solenoidal null space functions) that can be obtained through the SVD decomposition of $[Q_i^l]$, and $[0]$ is a null vector of dimension $(N_i^{l-1} - M_i^{l-1} + 1)$. Solving the system (24), the coefficients $f_{i,n}^l$ of (14) are found. Then, applying (14) recursively, any level-l generalized function $f_i^l(\mathbf{r})$ can be expressed as a linear combination of basis functions at level-0 as follows:

$$\mathbf{f}_i^l(\mathbf{r}) = \sum_{k=1}^{N} f_{i,k}^{l,0}\, \mathbf{f}_k^0(\mathbf{r}) \tag{25}$$

where each coefficient $f_{i,k}^{l,0}$ represents the weighting coefficient for the input level-0 functions.

C. Multi-Resolution MB-RWG Functions

The procedure for generating multi-resolution MB-RWG functions is described below. The MR functions provide a set of bases capable of improving the spectral properties of the SIE system by separating the current into solenoidal and non-solenoidal parts in a hierarchical scheme. The properties and multilevel nature of these functions transform the matrix system into a robust and well-conditioned system capable of accurately handling multiscale features and very small details, in contrast to a generic quasi-Helmholtz decomposition.

A collection of functions can be defined at each level of the hierarchical mesh decomposition as a linear combination of generalized functions at this given level as

$$\mathbf{w}_i^l(\mathbf{r}) = \sum_{k=1}^{K_i^l} T_{i,k}^l\, \mathbf{f}_{\delta_i(k)}^l(\mathbf{r}) \tag{26}$$

where K_i^l is the number of $\mathbf{f}_{\delta_i(k)}^l(\mathbf{r})$ functions defined inside the domain of $\mathbf{w}_i^l$, δ_i is the vector containing the global index of the level-l functions where $\mathbf{w}_i^l(\mathbf{r})$ is defined and $T_{i,k}^l$ are the weighting coefficients of each $\mathbf{f}_{\delta_i(k)}^l(\mathbf{r})$ function.

The first step to build the MR functions is the generation of the charge matrices in (16) for each group of children level-l cells belonging to a given level-$(l+1)$ cell. Then, the coefficients $T_{i,k}^l$ for non-solenoidal functions are determined by the non-zero singular vectors of the charge matrix, while the null singular vectors correspond to the coefficients of the solenoidal functions. To complete the solenoidal part, the divergence-free functions defined across each pair of adjacent level-$(l+1)$ cells must be added [44]. This set can be extracted from the null space functions of the joint charge matrix for the cells defining each generalized MB-RWG function on the level-$(l+1)$ mesh and subtracting the function space generated at the previous step by the Gram-Schmidt orthogonalization process.

A generic MR function $\mathbf{w}_i^l$ of level-l is expressed in (26) as linear combination of the generalized basis functions of the same level. Importantly, considering that all generalized functions at any level can be expressed as linear combinations of the original input MB-RWG and RWG functions (level-0), any generic level-l MR function can also be described as a linear combination of the input basis functions. So (26) can be express as follows:

$$\mathbf{w}_i^l(\mathbf{r}) = \sum_{k=1}^{N} T_{i,k}^{l,0}\, \mathbf{f}_k^0(\mathbf{r}) \tag{27}$$

where each coefficient $T_{i,k}^{l,0}$ represents the weighting coefficient for the input level-0 functions, which can be collected for each level as

$$\left[T^l\right] = \begin{bmatrix} T_{1,1}^{l,0} & T_{1,2}^{l,0} & \cdots & T_{1,N}^{l,0} \\ T_{2,1}^{l,0} & T_{2,2}^{l,0} & \cdots & T_{2,N}^{l,0} \\ \vdots & \vdots & \ddots & \vdots \\ T_{N_{\text{MR}}^l,1}^{l,0} & T_{N_{\text{MR}}^l,2}^{l,0} & \cdots & T_{N_{\text{MR}}^l,N}^{l,0} \end{bmatrix} \tag{28}$$

being N_{MR}^l the number of MR basis defined on level-l. The above $[T^l]$ matrices for each level can be put together to obtain a square MR change-of-basis matrix $[T_{\text{MR}}]$, since $N_{\text{MR}}^0 + N_{\text{MR}}^1 + \ldots, N_{\text{MR}}^{L-1} = N$, as

$$[T_{\text{MR}}] = \begin{bmatrix} [T^0] \\ [T^1] \\ \vdots \\ [T^{L-1}] \end{bmatrix} \tag{29}$$

paving the way for the application of the multilevel MR basis functions set as left and right multiplicative preconditioner of the original system, which can be easily combined with any fast SIE method [46].

As detailed in Sect. III-A, the above change-of-basis matrix (29) is applied when all level-$(L-1)$ cells are completely included in one level-L cell only. Notwithstanding, when structures with large electrical size come into play, the MR grouping procedure is stopped at the quasi-Nyquist cell-size level. The MR generation scheme is then applied for the first $(L-1)$ levels, while the generalized MB-RWG functions (Sect. III-B) defined at the last (coarsest) level-L (25) are included to complete the new set of functions, defining the corresponding change-of-basis matrix $[T_{\text{gf}}]$ as:

$$[T_{\text{gf}}] = \begin{bmatrix} f_{1,1}^{L,0} & f_{1,2}^{L,0} & \cdots & f_{1,N}^{L,0} \\ f_{2,1}^{L,0} & f_{2,2}^{L,0} & \cdots & f_{2,N}^{L,0} \\ \vdots & \vdots & \ddots & \vdots \\ f_{N_{\text{gf}}^L,1}^{L,0} & f_{N_{\text{gf}}^L,2}^{L,0} & \cdots & f_{N_{\text{gf}}^L,N}^{L,0} \end{bmatrix} \tag{30}$$

being N_{gf}^L the number of generalized basis functions defined on level-L. Note that $N_{\text{MR}}^0 + N_{\text{MR}}^1 + \ldots, N_{\text{MR}}^{L-1} + N_{\text{gf}}^L = N$.

The complete change-of-basis matrix $[T]$ can be then defined in terms of (29) and (30) as

$$[T] = \begin{bmatrix} [T_{\rm MR}] \\ [T_{\rm gf}] \end{bmatrix}. \tag{31}$$

with dimension $N \times N$. Note that if all the structure is included in one level-L cell only, $N_{\rm gf} = 0$ and $[T] = [T_{\rm MR}]$.

D. Complexity

As mentioned in previous sections, the most expensive operation in the generation of the proposed preconditioner is the SVD decomposition needed to find the coefficients of the solenoidal and non solenoidal bases. Applying the hierarchical decomposition of the input mesh, the dimension of the charge matrices is independent of the total number of unkowns (N), reducing the complexity of the algorithm up to $O(N \log N)$, where $\log N$ corresponds to the number of levels. The hierarchical nature of the MR basis functions limits the number of original basis that an MR depends to those defined on triangles belonging to the level-$l+1$ parent cells. Then, the change-of-basis matrix is sparse, allowing an efficient application of the MR preconditioner to the original system through parallel algorithms for sparse computation. The complexity of the generation algorithm is shown in Fig. 3 for the case of a sphere subdivided into eight symmetrical parts, with non-conformal meshes in the contours between them.

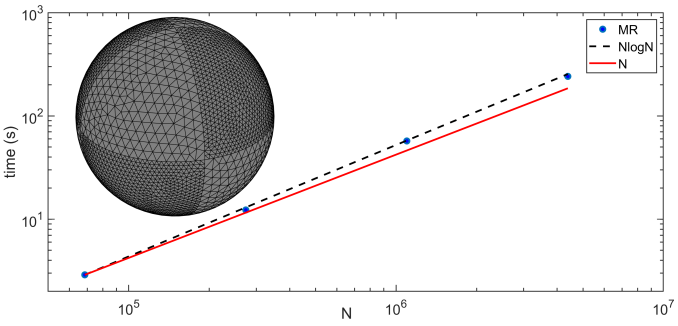

Fig. 3. Time to generate the multi-resolution basis versus the number of unknowns N. Case of a sphere subdivided into eight symmetrical parts, with non-conformal meshes, as shown in the inset.

E. Parallel implementation

A novel aspect of this work is also the introduction of a parallel implementation to take advantage of the availability of large multicore shared-memory computers in the generation of the MR basis functions. The proposed implementation relies on the use of the OpenMP standard under the C++ programming language. It aims to optimize parallel efficiency by adopting a two-step strategy. In a first step, the macro-cells of each level are calculated following the procedures of Sect. III-A, as described below highlighting the parallel implementation parts.

- The iterative grouping algorithm is applied sequentially to derive the cells and domains of the generalized basis functions of level-$(l+1)$ from the cells and domains of the generalized basis functions of level-l. The metrics and sets of possible next central cells are properly updated in each iteration, minimizing the number of dependencies between consecutive levels while keeping data locality and computational cost under control.
- Load balancing between parallel processes is a major concern for parallel efficiency. A load balancing algorithm is applied here to avoid large disparity in the number of children cells. Those macro-cells with a very small number of children compared to the neighboring cells are eliminated, and their children are relocated to the neighboring macro-cells with fewer number of children.
- A parallel loop by cells and domains of generalized functions is included next to precompute all the data needed for the generation of basis functions during the next step: topological relationships between cells and domains across the different levels, global and local indexing lists, sizes, lengths, etc.

Then, the procedures described in Sects. III-B and III-C are applied to derive the coefficients of the generalized and MR basis functions and the set of solenoidal and non-solenoidal functions. This is a complex part of the algorithm, and the one that benefits the most from the parallel implementation. This implementation is described below:

- A first parallel loop per macro-cells is included for the generation of the MR basis functions. The required charge matrices and SVD decomposition at level-$(l+1)$ are constructed from their children cells at level-l and solved to derive solenoidal and non-solenoidal basis functions. The load balancing scheme previously described in the generation of macro-cells is key to limit the size of these matrices, which can be directly calculated and factorized, while optimizing the parallel efficiency of the procedure. Note that this step does not include the calculation of solenoidal functions defined across pairs of adjacent cells, which are otherwise needed as indicated in Sect. III-C. Such divergence-free functions, defined on pairs of adjacent cells, will be calculated together with the generalized functions in the next parallel loop.
- The coefficients of the generalized basis functions and the set of divergence-free MR basis functions required to complete the solenoidal part, both defined on pairs of adjacent cells, are calculated in a second parallel loop. The required joint charge matrices and SVD decomposition at level-$(l+1)$ are constructed from their children cells at level-l, solved and orthogonalized through the Gram-Schmidt procedure, yielding the complete set of generalized, solenoidal, and non-solenoidal basis functions.

The above scheme provides a good scalability, which facilitates the parallel generation of the charge matrices and the MR functions, enabling the application of this method to real-life large-scale complex problems.

F. MoM solver

Once the construction of the MR change-of-basis matrix (31) is completed, the MoM system matrix (10) can be

transformed into a new system, expressed in the new function space, by applying the proposed approach as a multiplicative preconditioner, as follows:

$$\left[\hat{Z}\right] = [T] \cdot [Z] \cdot [T]^T \tag{32}$$

Next, two additional preconditioners are included to improve conditioning of the new system. First, a Jacobi diagonal preconditioner [47] $[D]$ is applied (both left and right) to the complete set of basis, where the non-zero elements (diagonal) of $[D]$ are given by

$$D_{ii} = \frac{1}{\sqrt{\hat{Z}_{ii}}} \tag{33}$$

with $i = 1, \ldots, N$. Second, an incomplete LU preconditioner is applied to the impedance matrix block corresponding to the generalized functions (after the Jacobi diagonal preconditioner), where $[L] \cdot [U] \approx [D_{\text{gf}}] \cdot \left[\hat{Z}_{\text{gf}}\right] \cdot [D_{\text{gf}}]$, being $\left[\hat{Z}_{\text{gf}}\right]$ and $[D_{\text{gf}}]$ the submatrices in (32) and (33) corresponding to the generalized functions [46].

The solution of the proposed SIE matrix system is accelerated considering an iterative parallel solver and a geometrical octree decomposition in space via the multilevel fast multipole algorithm with fast fourier transform (MLFMA-FFT) [3], [48]–[52]. As previously mentioned, the proposed MR approach is then embedded in the matrix system solution as a multiplicative preconditioner. Taking advantage of the local dependencies of the MR functions, a sparse change-of-basis matrix is defined to efficiently compute the preconditioning step through two sparse matrix vector products (SpMVP) before and after the MLFMA-FFT main matrix vector product (MVP). The interested reader is referred to [46] for more details on the implementation.

IV. Numerical Results

In this section, we illustrate the correctness and effectiveness of the proposed multi-resolution preconditioner in solving large-scale non-conforming meshed problems with real-life interest.

A. Validation example

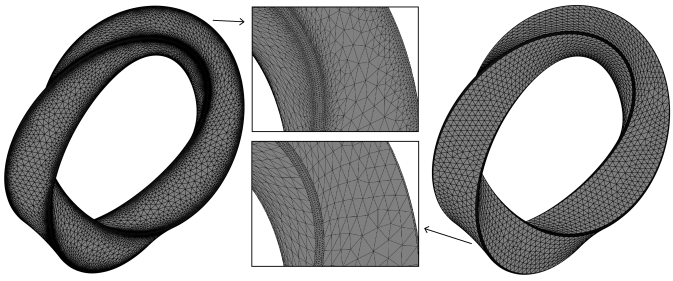

Fig. 4. Conformal (left) vs non-conformal (right) meshes of the Möbius strip.

A first numerical example is introduced to validate the proposed approach for the automatic generation of all solenoidal and non-solenoidal functions in the solution of a small object

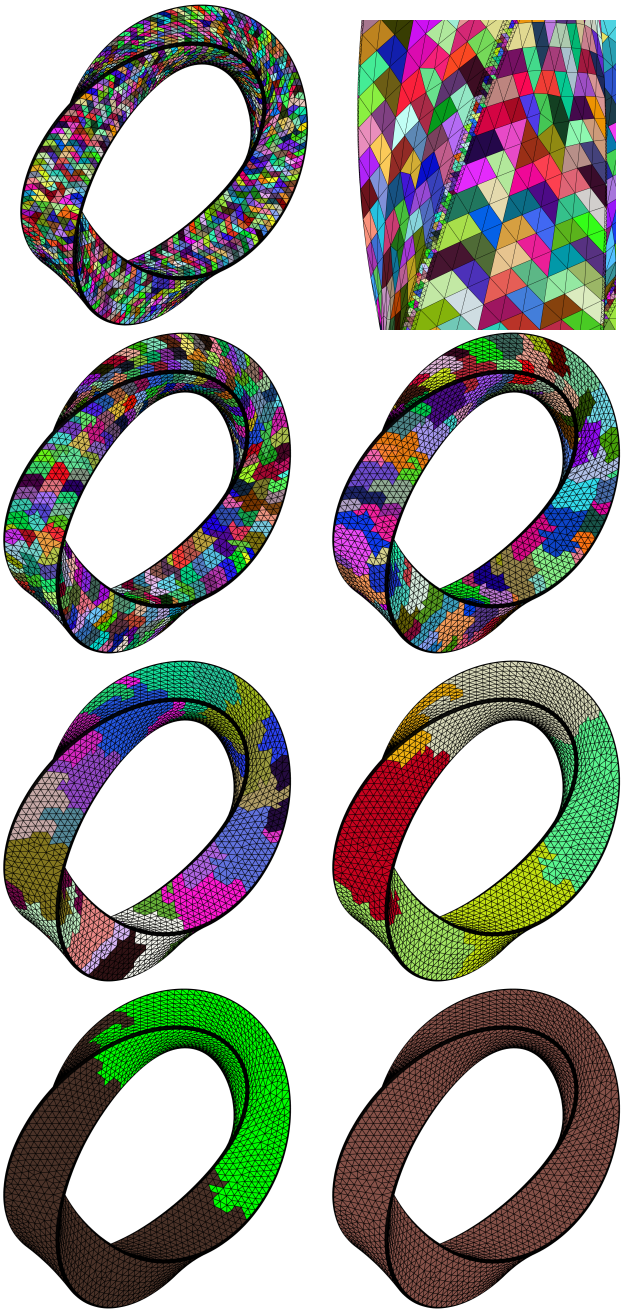

Fig. 5. Multi-level cell grouping algorithm for the Möbius strip.

containing global loops. A Möbius volumetric belt is considered, formed by three Möbius strips connected to each other by three small curved bands, forming a smooth curvature in the wedges (with a diameter of curvature of $\lambda/15$ and strip width of $\lambda/75$), as shown in Fig. 4. The surfaces that form this structure can be meshed independently, yielding non-conformal meshes at the junctions between them (see Fig. 4, on the right). The smooth strips are meshed with $\lambda/300$ triangular elements, while the three curved bands placed on the wedges are meshed with $\lambda/1500$ triangular size to minimize the geometrical discretization error on the curved wedges. The use of non-conformal meshes allows a drastic reduction in the number of unknowns, by removing the transition regions that

would be required in the case of the equivalent conformed mesh, as illustrated in Fig. 4 on the left. Consequently, the total number of unknowns reduces from 84,180 RWGs, in the conformal mesh case, to 33,033 RWGs plus 720 MB-RWGs.

We first examine the generation of the quasi-Helmholtz decomposition. The input mesh has 23,702 triangles (M), 10,051 inner nodes, V_{int}, (excluding MB-RWG internal nodes), and one structural handle (H). Figure 5 shows the cell grouping generated by the algorithm described in Sect. III-A, from level-1, where the input triangles are rearranged to provide the first generalized cells, to the last level, where all the input triangles are included in a single generalized cell. A detailed view of the level-1 grouping in the vicinity of the non-conformal meshes is shown in the upper right corner of Fig. 5.

The proposed multi-resolution generation scheme is then applied to each level-l mesh, automatically posing 10.052 solenoidal functions (N_s), and 23.701 non-solenoidal functions (N_{ns}), spread across the 7 levels of the grouping. These numbers match the required relationship between the number of non-solenoidal functions ($N_{ns} = M - 1$), and solenoidal functions ($N_s = V_{int} - 1 + 2H$), including the topological (global) loops corresponding to the handle, automatically generated via the proposed multi-level scheme.

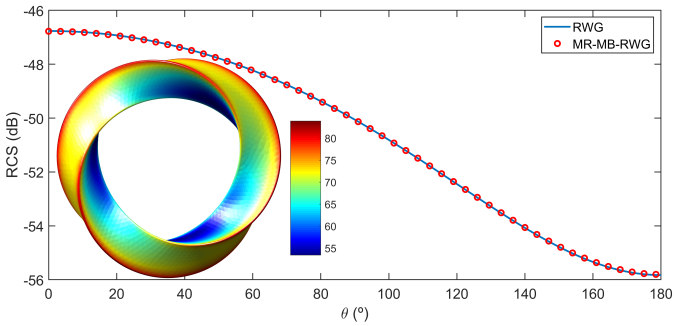

Fig. 6. Bistatic radar cross section and equivalent electric current density of the mobius strip ($dB\mu A/m$) at 300 MHz.

The bistatic radar cross section (RCS) is evaluated at 300 MHz for this example using the proposed MR preconditioner, grown from the RWG and MB-RWG basis functions. The result is depicted in Fig. 6, compared to the reference MoM solution using the conformally meshed structure of Fig. 4 on the left. A perfect agreement is observed between the MR-MB approach and the reference solution. The equivalent electric currents on the Möbius surfaces are shown in the inset of Fig. 6.

Figure 7 shows the convergence of the proposed approach in terms of the iteration number under an iterative Krylov resolution of the matrix system (we are using GMRES [53]). We can be observe that the MR preconditioner applied to non-conformal meshes outperforms the MB-RWG solution alone, without preconditioner, despite the small electrical size of the object. This reveals the effectiveness of the MR preconditioner applied to non-conformal meshes thought multi-branch basis functions.

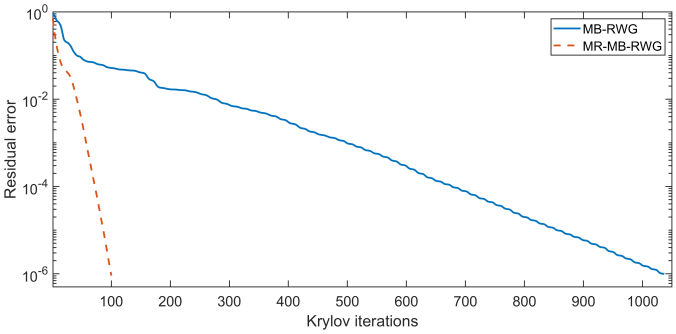

Fig. 7. Iteration count for the mobius strip considering a plane wave excitation.

B. Realistic multi-scale radiation example

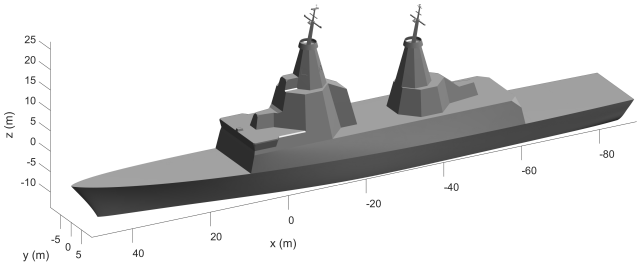

Fig. 8. Realistic vessel model.

A second numerical example is introduced to highlight the ability and versatility of the proposed approach to solve challenging multi-scale problems using non-conformal meshes. The evaluation of the isolation between the antennas of a ship-to-air communication system onboard a realistic vessel (shown in Fig. 8) is considered. The dimensions of the vessel are approximately 140 m length, 20 m beam and 40 m height ($257\lambda \times 36\lambda \times 74\lambda$ at the highest frequency, 550 MHz). The system consists of one or more transceivers connected to four patch antennas, which are built into the mid level of the main mast. The antennas are meshed separately, with a mesh size tailored to the fine detail features of their respective structures, and placed on the platform mesh resulting in non-conforming triangles on either side of the tear (connection) lines. Some details of the resulting mesh are illustrated in Fig. 9. The non-conformal mesh procedure leads to a total of 13,782,364 RWGs on the conformal-mesh surfaces, and 3,468 MB-RWGs in the tear lines connecting different parts of the structure. Regarding the MR functions, in this example, the multi-level mesh grouping algorithm is stopped at the quasi-Nyquist level (macro-cell size equal to around $\lambda/4$), providing a total of 3,514,716 solenoidal, 8,571,690 non-solenoidal, and 1,699,426 generalized RWG basis functions that complete the set of required basis functions. It is worth mentioning that this process keeps the same number of degrees of freedom as the original MB-RWG discretization, despite the levels truncated from the MR generation process. The problem is solved via the MLFMA applying the proposed MR-MB preconditioner together with the diagonal preconditioner.

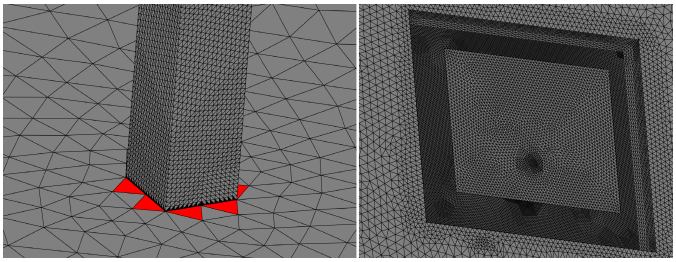

Fig. 9. Non-conformal mesh details of the feeding point and the connections of antennas with the structure.

Delta-gap voltage sources at the feed terminals are defined along the perimeter of the feed wires to simulate the radiation of the antenna system at a frequency of 550 MHz. This is illustrated on the left side of Fig. 9, depicting the positive (red) and negative (black) triangles of each excited basis function around the gap. Remarkably, MB-RWG basis functions are being considered as feeder terminals, for which the voltage value must be weighted by the length of the common edge of the positive triangle at each basis.

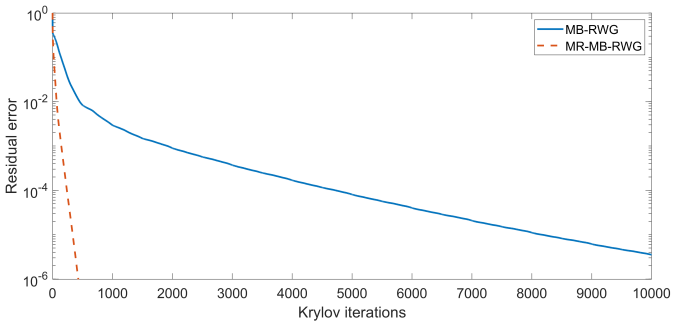

Fig. 10. Iteration count for the vessel considering a delta-gap excitation at 550 MHz.

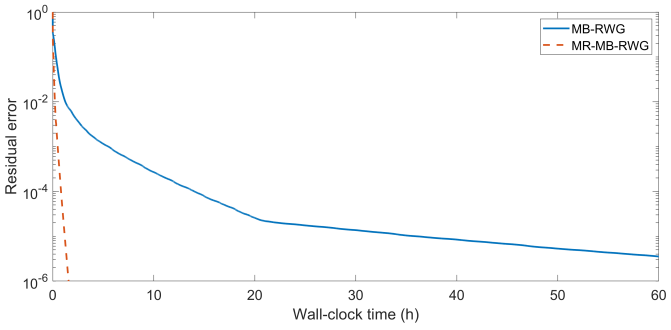

Fig. 11. Total time to solve the vessel considering a delta-gap excitation at 550 MHz.

Figure 10 compares the number of iterations in the solution process using the MR preconditioner and the original MB-RWG system with a left Jacobi diagonal preconditioner (33). It is evident the converge acceleration due to the applied MR-MB preconditioner, which takes less than 500 iterations to converge to a residual error of $9.8 \cdot 10^{-7}$, in contrast to the more than 10000 iterations spent by MB-RWG to reach a residual error of $3.6 \cdot 10^{-6}$. Regarding the wall-clock per iteration 11, the MR preconditioner can be included as a multiplicative preconditioner that only need the inclusion of two additional sparse matrix vector product (MVP) [46] without a significant reduction of performance in comparison with the original MVP in the case of large-scale problems, achieving the expected accuracy in 1.5 hours in contrast to the more than 60 hours spent by the Jacobi preconditioner.

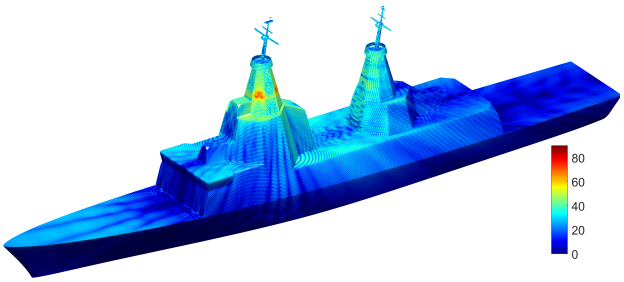

Fig. 12. Equivalent electric current density ($dB\mu A/m$) induced on the vessel surfaces at 550 MHz.

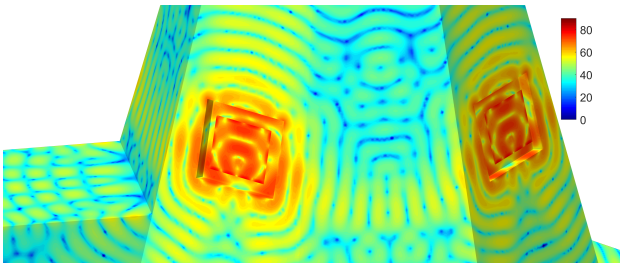

Fig. 13. Equivalent electric current density ($dB\mu A/m$) induced on the vessel surfaces, close to the radiating antenna, at 550 MHz.

Figure 12 reports the obtained equivalent electric current densities induced on the ship surfaces at 550 MHz. The noiseless distribution of current and the absence of artefacts on the tearing lines between non-conformal discretizations are shown in the detailed view of one antenna (see Fig. 13).

To end this example, the mutual coupling study of the HF system antennas is obtained by a frequency sweep simulation from 100 MHz to 550 MHz. Figure 14(a) shows the amplitude of the S_{i3} parameters, for $i = 1$, 2 and 4, accounting for the mutual coupling between the antenna no. 3 and the rest of the onboard antennas conforming the communication system. Furthermore, Fig. 14(b) shows the self coupling ($|S_{33}|$) parameter. Figure 14 also compares the S_{i3} parameters obtained with the reference MLFMA problem applied to the equivalent conformal meshed problem, where mesh transition regions are needed to adapt the different mesh densities. A good agreement between the proposed MR-MB results and the reference can be observed.

C. H-refinement multi-scale scattering example

A different example is shown next. Up to now the focus of using MB has been in transitions between different sections of a complex geometry. In this example, the usefulness of the

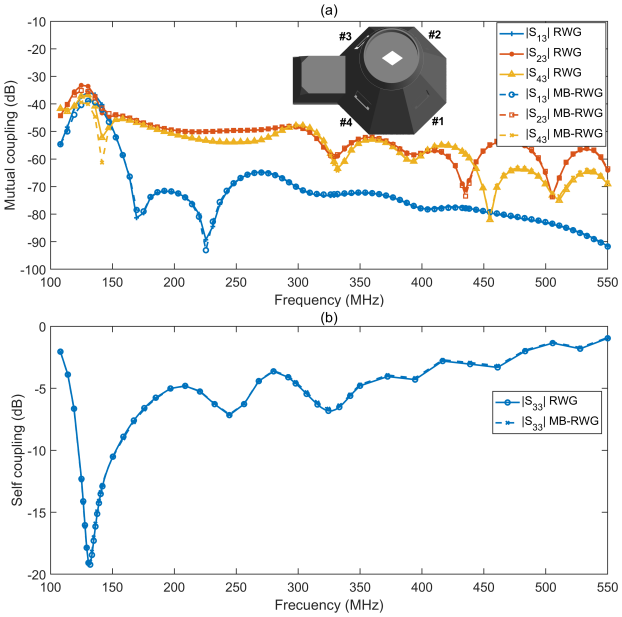

Fig. 14. Mutual (a) and self (b) coupling ($|S_{i3}|$) for the transmitting patch antenna no. 3 in the frequency range from 100 to 550 MHz.

proposed approach is demonstrated in the application of h-refinement techniques, which allow increasing the degrees of freedom in those regions where there are fine geometric details or where higher precision is required. This naturally gives rise to non-conforming multi-scale problems with localized mesh refinement.

The scattering of a morphed version of a Rafale aircraft is considered. An automatic h-refinement method [11] is applied to the input mesh, with two steps of refinement, rendering a locally refined version that improves accuracy without burdening the computational cost. The final mesh obtained and the first MR grouping level are shown in Figs. 15 and 16, respectively. The maximum length of the aircraft is 7λ at the working frequency, 137 MHz, and the problem is modeled using 55,267 RWG basis functions in the conformal-mesh regions and 4,543 MB-RWG basis functions in the non-conformal mesh parts of the geometry.

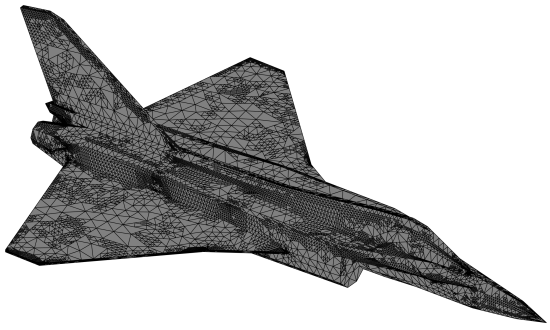

Fig. 15. H-refinement non-conformal mesh of the Rafale aircraft .

Figures 17 and 18 compares the GMRES residual error of the proposed MR-MB basis with respect to the initial MB and RWG basis using the MLFMA for the solution of the problem

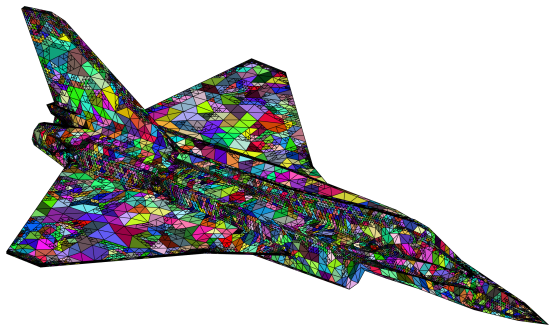

Fig. 16. MR grouping in the first mesh level of the Rafale aircraft.

with a plane wave excitation. It can be observed looking at these figures that the combination of the MR preconditioner with the MB-RWG basis functions drastically reduces both the global number of iterations and the total simulation time, achieving a Krylov residual error below 10^{-6} in just 140 iterations and 10 seconds.

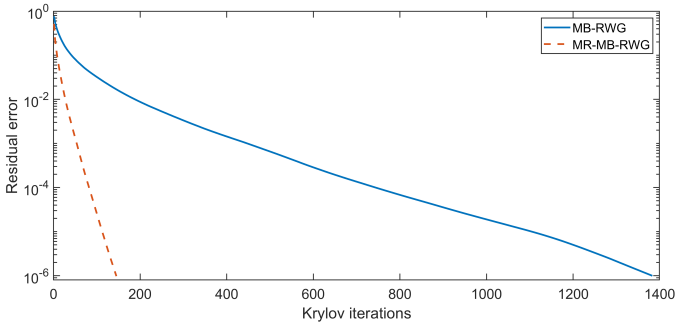

Fig. 17. Iteration count for the aircraft considering a plane wave excitation.

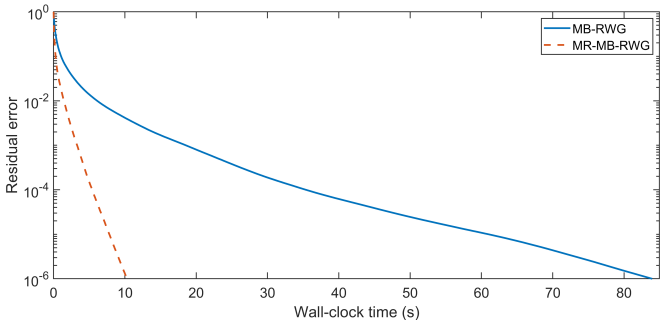

Fig. 18. Total time to solve the aircraft considering a plane wave excitation.

Finally, the equivalent currents distribution in the aircraft structure at 137 MHz are shown in Fig. 19.

V. Conclusion and Perspectives

In this work, the multi-resolution preconditioner was combined with the multi-branch RWG functions, enabling the application of an automatic multilevel quasi-Helmholtz decomposition for the first time to the electromagnetic analysis of non-conformal meshed objects including multi-scale features.

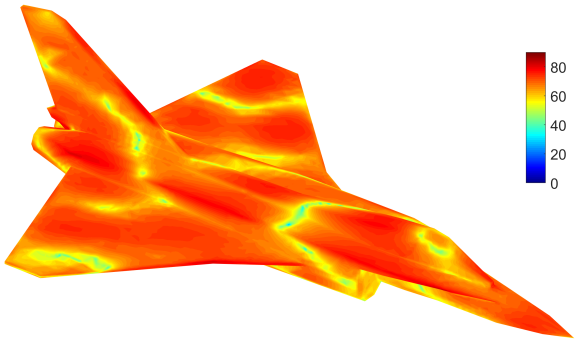

Fig. 19. Equivalent electric current density ($dB\mu A/m$) induced on the aircraft surfaces.

The div-conforming property of multi-branch RWG basis functions allows the quasi-Helmholtz decomposition applied to non-conformal meshes. This provides an efficient, accurate and versatile solver for dealing with very large-scale and extremely complex geometries due to the multilevel nature of the proposed method. The efficiency and versatility of the proposed approach has been demonstrated for the solution of very small scattering problems and really large-scale radiation and problems including multi-scale details. The proposed method has also been demonstrated as a powerful solver for the application of h-refinement techniques in the case of problems including deep multi-scale features.

In addition, it is important to note that the MR-MB method is presented as a strong candidate to be integrated into a domain decomposition scheme in order to speed up the solution of the mutual coupling between subdomains in the case of extremely complex subdomains with multi-scale features.

REFERENCES

[1] R. F. Harrington, *Field Computation by Moment Method*. NJ, USA: IEEE Press, 1993.

[2] A. Poggio and E. Miller, "Integral Equation Solutions of Three-dimensional Scattering Problems," in *Computer Techniques for Electromagnetics*. Elsevier, 1973, pp. 159–264.

[3] W. C. Chew, J.-M. Jin, E. Michielssen, and J. M. Song, Eds., *Fast and Efficient Algorithms in Computational Electromagnetics*. Norwood, MA, USA: Artech House, 2001.

[4] B. M. Kolundzija and A. R. Djordjevic, *Electromagnetic Modeling of Composite Metallic and Dielectric Structures*. Norwood, MA, USA: Artech House, 2002.

[5] P. Ylä-Oijala and M. and Taskinen, "Application of combined field integral equation for electromagnetic scattering by dielectric and composite objects," *IEEE Transactions on Antennas and Propagation*, vol. 53, no. 3, pp. 1168–1173, mar 2005.

[6] F. Andriulli, K. Cools, F. Olyslager, A. Buffa, S. Christiansen, and E. Michielssen, "A multiplicative Calderon preconditioner for the electric field integral equation," *IEEE Transactions on Antennas and Propagation*, vol. 56, no. 8, pp. 2398–2412, aug 2008.

[7] Ö. Ergül and L. Gürel, "Comparison of integral-equation formulations for the fast and accurate solution of scattering problems involving dielectric objects with the multilevel fast multipole algorithm," *IEEE Transactions on Antennas and Propagation*, vol. 57, no. 1, pp. 176–187, jan 2009.

[8] F. Vipiana, M. A. Francavilla, and G. Vecchi, "EFIE modeling of highdefinition multiscale structures," *IEEE Transactions on Antennas and Propagation*, vol. 58, no. 7, pp. 2362–2374, jul 2010.

[9] Z. Peng, K. H. Lim, and J. F. Lee, "Computations of electromagnetic wave scattering from penetrable composite targets using a surface integral equation method with multiple traces," *IEEE Transactions on Antennas and Propagation*, vol. 61, no. 1, pp. 256–269, jan 2013.

[10] J.-M. Jin, *Theory and Computational Electromagnetic Fields, 2nd ed.* Hoboken, NJ, USA: Wiley, 2015.

[11] J. A. Tobon Vasquez, Z. Peng, J.-F. Lee, G. Vecchi, and F. Vipiana, " Automatic Localized Nonconformal Mesh Refinement for Surface Integral Equations," *IEEE Transactions on Antennas and Propagation*, vol. 68, no. 2, pp. 967–975, 2020.

[12] Z. Peng, K. H. Lim, and J. F. Lee, "A discontinuous galerkin surface integral equation method for electromagnetic wave scattering from non-penetrable targets," *IEEE Transactions on Antennas and Propagation*, vol. 61, no. 7, pp. 3617–3628, 2013.

[13] M. A. Echeverri Bautista, F. Vipiana, M. A. Francavilla, J. A. Tobon Vasquez, and G. Vecchi, "A nonconformal domain decomposition scheme for the analysis of multiscale structures," *IEEE Transactions on Antennas and Propagation*, vol. 63, no. 8, pp. 3548–3560, 2015.

[14] Z. Peng, R. Hiptmair, Y. Shao, and B. MacKie-Mason, "Domain decomposition preconditioning for surface integral equations in solving challenging electromagnetic scattering problems," *IEEE Transactions on Antennas and Propagation*, vol. 64, no. 1, pp. 210–223, jan 2016.

[15] G. Xiao and Y. Hou, "Intuitive formulation of discontinuous galerkin surface integral equations for electromagnetic scattering problems," *IEEE Transactions on Antennas and Propagation*, vol. 65, no. 1, pp. 287–294, 2017.

[16] Y. Chen, D. Li, J. Hu, and J. F. Lee, "A nonconformal surface integral equation for electromagnetic scattering by multiscale conducting objects," *IEEE Journal on Multiscale and Multiphysics Computational Techniques*, vol. 3, pp. 225–234, 2018.

[17] B. B. Kong and X. Q. Sheng, "A Discontinuous Galerkin Surface Integral Equation Method for Scattering from Multiscale Homogeneous Objects," *IEEE Transactions on Antennas and Propagation*, vol. 66, no. 4, pp. 1937–1946, apr 2018.

[18] E. Ubeda and J. M. Rius, "Novel monopolar MFIE MoM-discretization for the scattering analysis of small objects," *IEEE Transactions on Antennas and Propagation*, vol. 54, no. 1, pp. 50–57, 2006.

[19] E. Ubeda, J. M. Rius, and A. Heldring, "Nonconforming discretization of the electric-field integral equation for closed perfectly conducting objects," *IEEE Transactions on Antennas and Propagation*, vol. 62, no. 8, pp. 4171–4186, 2014.

[20] E. Ubeda, J. M. Rius, A. Heldring, and I. Sekulic, "Volumetric Testing Parallel to the Boundary Surface for a Nonconforming Discretization of the Electric-Field Integral Equation," *IEEE Transactions on Antennas and Propagation*, vol. 63, no. 7, pp. 3286–3291, 2015.

[21] E. Ubeda, I. Sekulic, J. M. Rius, and A. Heldring, " Tangential-Normal Surface Testing for the Nonconforming Discretization of the Electric-Field Integral Equation," *IEEE Antennas and Wireless Propagation Letters*, vol. 15, pp. 1581–1584, 2016.

[22] I. Sekulic, D. C. Tzarouchis, P. Ylä-Oijala, E. Ubeda, and J. M. Rius, "Enhanced discretization of surface integral equations for resonant scattering analysis of sharp-edged plasmonic nanoparticles," *Physical Review B*, vol. 99, no. 16, p. 165417, 2019.

[23] I. Sekulic, E. Ubeda, and J. M. Rius, "Versatile and accurate schemes of discretization for the electromagnetic scattering analysis of arbitrarily shaped piecewise homogeneous objects," *Journal of Computational Physics*, vol. 374, pp. 478–494, 2018.

[24] S. Huang, G. Xiao, Y. Hu, R. Liu, and J. Mao, "Multibranch Rao–Wilton–Glisson Basis Functions for Electromagnetic Scattering Problems," *IEEE Transactions on Antennas and Propagation*, vol. 69, no. 10, pp. 6624–6634, 2021.

[25] S. Huang, G. Xiao, Y. Hu, and R. Liu, "Loop star functions including multibranch rao-wilton-glisson basis functions," *IEEE Transactions on Antennas and Propagation*, vol. 70, no. 5, pp. 3910–3915, 2022.

[26] F. P. Andriulli, K. Cools, H. Bagci, F. Olyslager, A. Buffa, S. Christiansen, and E. Michielssen, "A Multiplicative Calderon Preconditioner for the Electric Field Integral Equation," *IEEE Transactions on Antennas and Propagation*, vol. 56, no. 8, pp. 2398–2412, 2008.

[27] H. Contopanagos, B. Dembart, M. Epton, J. Ottusch, V. Rokhlin, J. Visher, and S. Wandzura, "Well-conditioned boundary integral equations for three-dimensional electromagnetic scattering," *IEEE Transactions on Antennas and Propagation*, vol. 50, no. 12, pp. 1824–1830, 2002.

[28] R. Adams, "Physical and analytical properties of a stabilized electric field integral equation," *IEEE Transactions on Antennas and Propagation*, vol. 52, no. 2, pp. 362–372, 2004.

[29] M. B. Stephanson and J.-F. Lee, "Preconditioned Electric Field Integral Equation Using Calderon Identities and Dual Loop/Star Basis Functions," *IEEE Transactions on Antennas and Propagation*, vol. 57, no. 4, pp. 1274–1279, 2009.

[30] O. Bruno, T. Elling, R. Paffenroth, and C. Turc, "Electromagnetic integral equations requiring small numbers of Krylov-subspace iterations," *Journal of Computational Physics*, vol. 228, no. 17, pp. 6169–6183, 2009.
[31] S. H. Christiansen and J.-C. Nédélec, "A Preconditioner for the Electric Field Integral Equation Based on Calderon Formulas," *SIAM Journal on Numerical Analysis*, vol. 40, no. 3, pp. 1100–1135, 2002.
[32] F. P. Andriulli, F. Vipiana, and G. Vecchi, "Hierarchical Bases for Nonhierarchic 3-D Triangular Meshes," *IEEE Transactions on Antennas and Propagation*, vol. 56, no. 8, pp. 2288–2297, 2008.
[33] F. Vipiana, P. Pirinoli, and G. Vecchi, "A Multi-Resolution Method of Moments for Triangular Meshes," *IEEE Transactions on Antennas and Propagation*, vol. 53, no. 11, pp. 2247–2258, 2005.
[34] H. Chen, D. Ding, R. Chen, D. Wang, and E. K. Yung, "Application of multiresolution preconditioner technique for scattering problem in a half space," in *2008 International Conference on Microwave and Millimeter Wave Technology*, vol. 2, 2008, pp. 975–977.
[35] J. J. Ding, J. Zhu, D. Ding, R. S. Chen, D. Wang, and E. K. Yung, "Application of perturbed multiresolution preconditioner technique combined with MLFMA for scattering problem," in *2008 International Conference on Microwave and Millimeter Wave Technology*, vol. 2, 2008, pp. 978–981.
[36] D. Wen, Y. Wang, L. Liu, and Z. Nie, "Improved Multiresolution Preconditioner With Loop-Flower Basis Functions," *IEEE Antennas and Wireless Propagation Letters*, vol. 16, pp. 1349–1352, 2017.
[37] R.-S. Chen, J. Ding, D. Z. Ding, Z. H. Fan, and D. Wang, "A Multiresolution Curvilinear Rao–Wilton–Glisson Basis Function for Fast Analysis of Electromagnetic Scattering," *IEEE Transactions on Antennas and Propagation*, vol. 57, no. 10, pp. 3179–3188, 2009.
[38] M. A. Echeverri Bautista, M. A. Francavilla, F. Vipiana, and G. Vecchi, "A Hierarchical Fast Solver for EFIE-MoM Analysis of Multiscale Structures at Very Low Frequencies," *IEEE Transactions on Antennas and Propagation*, vol. 62, no. 3, pp. 1523–1528, 2014.
[39] M. A. Francavilla, F. Vipiana, G. Vecchi, and D. R. Wilton, "Hierarchical Fast MoM Solver for the Modeling of Large Multiscale Wire-Surface Structures," *IEEE Antennas and Wireless Propagation Letters*, vol. 11, pp. 1378–1381, 2012.
[40] F. Vipiana, P. Pirinoli, and G. Vecchi, "Spectral properties of the EFIE-MoM matrix for dense meshes with different types of bases," *IEEE Transactions on Antennas and Propagation*, vol. 55, no. 11, pp. 3229–3238, 2007.
[41] V. F. Martin, J. M. Taboada, and F. Vipiana, "A non-conformal multi-resolution preconditioner in the MoM solution of large multi-scale structures," in *2022 IEEE International Symposium on Antennas and Propagation and USNC-URSI Radio Science Meeting (AP-S/URSI)*, July 2022.
[42] V. F. Martín, J. M. Taboada, and F. Vipiana, "A non-conformal multi-resolution preconditioner in the MoM solution of large multi-scale structures," in *2022 International Conference on Electromagnetics in Advanced Applications (ICEAA)*, Sept 2022.
[43] S. M. Rao, D. R. Wilton, and A. W. Glisson, "Electromagnetic scattering by surfaces of arbitrary shape," *IEEE Transactions on Antennas and Propagation*, vol. 30, no. 3, pp. 409–418, may 1982.
[44] F. Vipiana and G. Vecchi, "A Novel, Symmetrical Solenoidal Basis for the MoM Analysis of Closed Surfaces," *IEEE Transactions on Antennas and Propagation*, vol. 57, no. 4, pp. 1294–1299, 2009.
[45] F. Vipiana, F. P. Andriulli, and G. Vecchi, "Two-tier non-simplex grid hierarchic basis for general 3D meshes," *Waves in Random and Complex Media*, vol. 19, no. 1, pp. 126–146, 2009.
[46] D. M. Solís, V. F. Martín, J. M. Taboada, and F. Vipiana, "Multiresolution Preconditioners for Solving Realistic Multi-Scale Complex Problems," *IEEE Access*, vol. 10, pp. 22 038–22 048, 2022.
[47] Saad, Yousef, *Iterative methods for sparse linear systems*. SIAM, 2003.
[48] J. Song, C.-C. Lu, and W. C. Chew, "Multilevel fast multipole algorithm for electromagnetic scattering by large complex objects," *IEEE Transactions on Antennas and Propagation*, vol. 45, no. 10, pp. 1488–1493, 1997.
[49] X. Sheng, J.-M. Jin, J. Song, W. Chew, and C.-C. Lu, "Solution of combined-field integral equation using multilevel fast multipole algorithm for scattering by homogeneous bodies," *IEEE Transactions on Antennas and Propagation*, vol. 46, no. 11, pp. 1718–1726, 1998.
[50] J. M. Taboada, M. Gomez-Araujo, J. M. Bertolo, L. Landesa, F. Obelleiro, and J. L. Rodriguez, "MLFMA-FFT Parallel Algorithm for the Solution of Large-Scale Problems in Electromagnetics (Invited Paper)," *Progress In Electromagnetics Research*, vol. 105, pp. 15–30, 2010.
[51] J. M. Taboada, M. G. Araujo, F. O. Basteiro, J. L. Rodriguez, and L. Landesa, "MLFMA-FFT parallel algorithm for the solution of extremely large problems in electromagnetics," *Proceedings of the IEEE*, vol. 101, no. 2, pp. 350–363, 2013.
[52] Kong, Wei-Bin and Zhou, Hou-Xing and Zheng, Kai-Lai and Hong, Wei, "Analysis of Multiscale Problems Using the MLFMA With the Assistance of the FFT-Based Method," *IEEE Transactions on Antennas and Propagation*, vol. 63, no. 9, pp. 4184–4188, 2015.
[53] Y. Saad and M. H. Schultz, "GMRES: A Generalized Minimal Residual Algorithm for Solving Nonsymmetric Linear Systems," *SIAM Journal on Scientific and Statistical Computing*, vol. 7, no. 3, pp. 856–869, 1986.

Víctor F. Martín received the M.S degrees in Telecommunication Engineering from the University of Extremadura (Spain) in 2019 and the Ph.D. degree in aerospace engineering with specialization in electromagnetics from the same university in 2022. He is currently working toward his postdoctoral researcher with the Dept. of Electronics at the Politecnico di Torino. His areas of interest include fast integral equation methods, domain decomposition techniques and supercomputing techniques in computational electromagnetics, electromagnetic compatibility, and analysis of nano-optical devices. He received the "Premio Liberalizacion de las Telecomunicaciones" award by the spanish COGITT for its B.S. thesis and the "Premio Extraordinario de Doctorado" award for his Ph.D thesis.

José M. Taboada was born in Pontevedra, Galicia, Spain, in 1974. He received the M.S. and Ph.D. degrees in telecommunication engineering from the University of Vigo, Spain, in 1998 and 2001, respectively. From 1998 to 2002, he worked as a researcher at the University of Vigo. In 2002, he joined the School of Technology, University of Extremadura, Spain, as an Associate Professor. He became Full Professor in 2019. His current research interests include integral-equation numerical methods in computational electromagnetics, with focus on fast solvers, domain decomposition techniques and parallel supercomputing, plasmonics, metamaterials and bio-sensing applications. He is also involved in the evaluation and control of electromagnetic compatibility and interference of cosite antennas and transceivers. He received the International PRACE Award and Intel Itanium Solutions Innovation Award in the year 2009 for their work in electromagnetics and supercomputing.

Francesca Vipiana received the Laurea and Ph.D. degrees in electronic engineering from the Politecnico di Torino, Torino, Italy, in 2000 and 2004, respectively, with doctoral research carried out partly at the European Space Research Technology Center, Noordwijk, The Netherlands. From 2005 to 2008, she was a Research Fellow with the Dept. of Electronics, Politecnico di Torino. From 2009 to 2012, she was the Head of the Antenna and EMC Laboratory, ISMB, Torino. Since 2012, she has been an Assistant Professor with the Dept. of Electronics, Politecnico di Torino, an Associate Professor since 2014 and a Full Professor since 2021. Her current research interests include numerical techniques based on the integral equation and method of moment approaches, with a focus on multiresolution and hierarchical schemes, domain decomposition, preconditioning and fast solution methods, and advanced quadrature integration schemes. She is currently involved in the modelling, design and testing of microwave imaging systems, for medical and industrial applications. She received the YS Award at the URSI GA in 2005, the First Prize in the Poster Competition at the IEEE Women in Electromagnetics Workshop in 2009, the ISMB Best Paper Award in 2011, and the Lot Shafai Mid-Career Distinguished Award from the IEEE APS in 2017.